CHAPTER 45

Experimental study on kinematics and dynamics of wave breaking

Masaru MIZUGUCHI[*]

1 Introduction
    Wave breaking on a slope is one of the most important problems for
the coastal engineers to be investigated. However wave breaking is a
complex phenomenon which is not yet fully understood, in spite of the
fact that many researches have been devoted to that subject. It is well
known that waves break in different forms: spilling, plunging and
surging.   Untill now no theoretical explanation is given for the
classification of the breaking pattern.   Recently numerical simulation
of wave breaking with full nonlinear governing equations based on the
irrotational assumption have been developed (Longuet-Higgins & Cokelet,
1976 and so on). The simulation results show that the spilling breaker
exhibit a small scale plunging jet as Miller (1976) observed in a
laboratory experiment.
    Most of the research works on the wave breaking are based on the
laboratory experiments, in particular visual observation. Basco(1985)
is the latest one on this line. Description of wave breaking based on
visual observations provide limited information. Hedge & Kirkgöz(1981)
report an experimental work in which the photographic approach was
supplemented by the velocity measurement by Laser- Doppler Velocimeter.
They found that the water particle velocity at the crest is smaller than
the wave crest propagation velocity especially on steep slope beaches,
and suggest that the plunging jet is not necessary formed at the crest.
It is normally accepted that the flow field is irrotational before waves
break. Therefore generation of vorticity as well as turbulence can be
considered as eminent features of the wave breaking. Few studies are
reported where velocity are measured in a fine grid of points so that
the vorticity can be evaluated (Okayasu et al., 1986). There are
several papers which pay an attention mainly on the structure of
turbulence induced by wave breaking (Peregrine & Svendsen, 1978, Stive,
1980 and so on.)
    Our aims are to provide a set of experimental data of a wave
breaking of plunging type on a slope, in which the velocity field is
measured in detail with high accuracy, and to discuss the kinematics and
dynamics based on the data set, especially from the inception of
breaking through the plunging process. In view of the initiation of
wave breaking, forming of the plunging jet or overturning may be
essential. Peregrine (1983) gives a comprehensive study of the fluid
dynamics of the wave breaking, in which some possiblities of the
plunging process are discussed.

2 Experiment
    The experiment was conducted in a laboratory wave flume of width 30
cm and of length 20 m. A wave of period 1.22 s and of wave height 4.4
cm at the uniform depth area of 28.2 cm deep was chosen, as it produced
a stable plunging breaker of height 6.1 cm at the depth of 6.5 cm on a

[*]Assoc. Prof., Dept. Civil Eng., Chuo Univ., Bunkyou-ku Tokyo 113 JAPAN

slope of 1/20. The slope is made of painted steel plate.

Wave profiles were measured by a capacitance-type wave gauge at offshore and by a specially designed resistance-type wire gauge (Masatoyo Kogaku) in the breaker zone. The latter gauge detects the top boundary between the air and the water. The wave gauge has higher frequency response ($\fallingdotseq$50 Hz for the amplitude of 25cm) and is better to detect the rapid change of the breaking wave profiles. First cross-shore (horizontal) and vertical velocities were measured at 126 points by using two-colour Laser-Doppler Velocimeter (DANTEC). Back scattering method was employed. Later second experiment was carried out, adding 132 measuring points mainly in the shallower and the deeper region. Unfortunately the incident waves were a little (4.5 cm of wave height) larger in the second run. The measuring area covers 112 cm horizontally, extending d=2.7 cm to d=8.3 cm, where d denotes the water depth. It covers the area vertically from the near-bottom to the wave crest level. The measuring section was located about 6 cm apart from the nearer
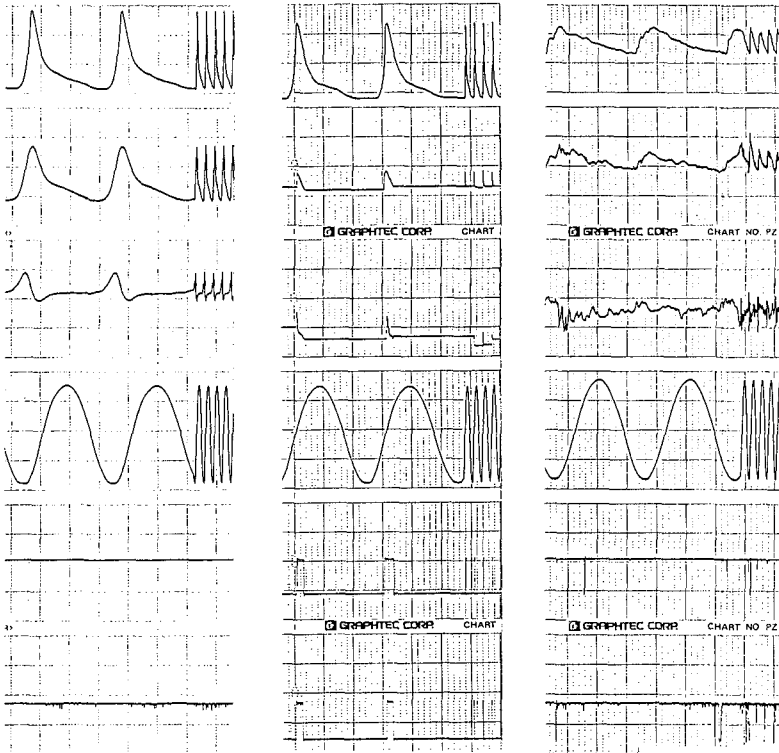
(a) d=7.5cm, z=-2.0cm   (b) d=6.6cm, z=2.0cm   (c) d=2.7cm, z=-0.8cm
Fig.1 Examples of raw data. Top, surface elevation by the wire gauge, Second, onshore velocity, u, by LDV, third, upward velocity, v, by LDV, fourth, surface elevation by CWG in uniform depth area, fifth, drop-out signal for u, bottom, drop-out signal for v. Vertical axis is not scaled. LDV signals hold the previous values while they drop out.
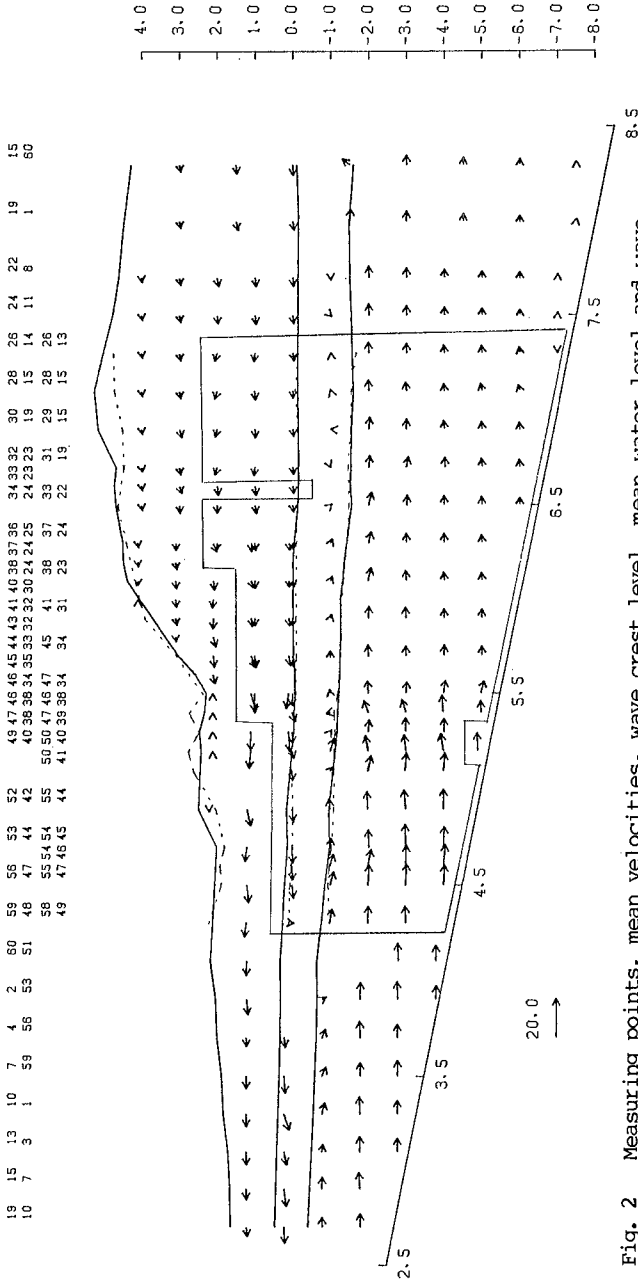
Fig. 2   Measuring points, mean velocities, wave crest level, mean water level and wave trough level. The measuring points within the solid line are for the first run. Some points above the still water level (z=0) were measured in both runs. The number at the top indicate the time by sequence number when the wave crest and trough pass the point. The number of the top two lines are for the second run. The dotted line for wave crest, mean water level and wave trough level are from the first run. The number below the bottom slope indicate the local water depth. Vertical axis is taken upward from the still water level. c.g.s. unit is used throughout the paper.

sidewall, which is made of glass.   To prevent the drop-out of LDV
signal, it is better to have the section nearer to the wall, although
the sidewall effects must be avoided.   The experimental data were
recorded on a magnetic tape and later digitized with a sampling
frequency of 50 Hz.
     In Fig. 1 (a)-(c), examples of raw data at various locations are
shown. Figure 2 shows the location of measuring points. The mean
velocity, mean water level, wave crest level and wave trough level are
also plotted in Fig.2. Mean water level, wave crest level and trough
level are obtained from the averaged wave profile of those at the points
in the same vertical section. It is seen that the total mass flux across
a vertical plane may not be zero and directed offshoreward. It is
because the LDV signals drop out giving zero velocities when the points,
above the trough level, just come into and out of the water as typically
shown in Fig. 1-(b). The Eulerian return flow, which compensate the wave
mass flux above the wave trough, exhibits uniform vertical distribution
after the plunging point. This uniform distribution is attributed to the
momentum transfer due to the strong turbulence in that region as shown
below.   Outside the breaking point the vertical distribution of the
return flow show a clear decrease toward the bottom.
     Representative temporal profiles of both surface elevation and
velocities for one period at each location were obtained by taking the
phase average values over the forty waves.   In the aerated area and the
near-surface area, the signals of LDV drop out frequently as shown in
Fig.1-(c).   When the signals obtained for no more than ten wave cycles
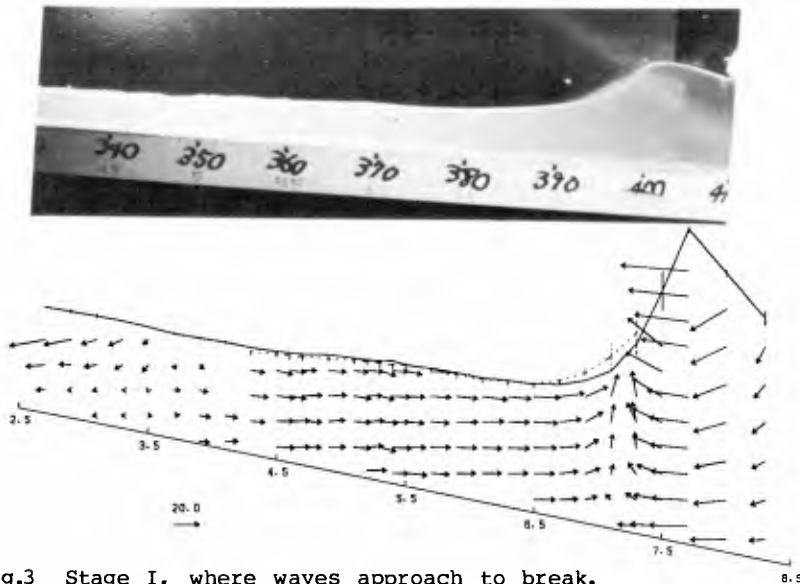among the forty, the data points for that phase were discarded.   Then

Fig.3   Stage I, where waves approach to break.
Photo and (phase averaged) velocity field. (T_i=22) The length of
vertical bars on the surface profile denote the standards error of the
wave profiles over the points on the same vertical section.   It
indicates the degree of fluctuation of the waves themselves.

the spatial distribution of the phase-averaged wave profile and velocities are produced by synthesizing the data of all measuring points. The synchronization was done by using the zero crossing point of the wave profiles measured at a fixed point of uniform depth area. Here the error of the order of a sampling time was inevitable. However larger error may occur when the data obtained in a second run and the data in the second run are brought together. These errors may be significant when the spatial derivatives are estimated as done below.

3 Analysis
     From the set of spatial distribution of phase averaged velocity, $\underline{u}$, the divergence, $\underline{\nabla}.\underline{u}$ and the rotation, $\underline{\nabla} x \underline{u}$ of the velocity vector field are calculated. The spatial derivatives of velocities are estimated by fitting a linear plane to the data of the points within an ellipse with a least square error. The ellipse has the horizontal radius $4r_0$ and vertical radius r_0. The value of r_0 is taken to be 1.6 cm. Theoretically the value should be infinitely small. The grid size in our experiments, however, requires a certain finite value. The values of 1.1, 1.3, and 2.1 cm were also tried. Only the results for the values of 2.1 cm produce considerably different distributions of derivatives. The water
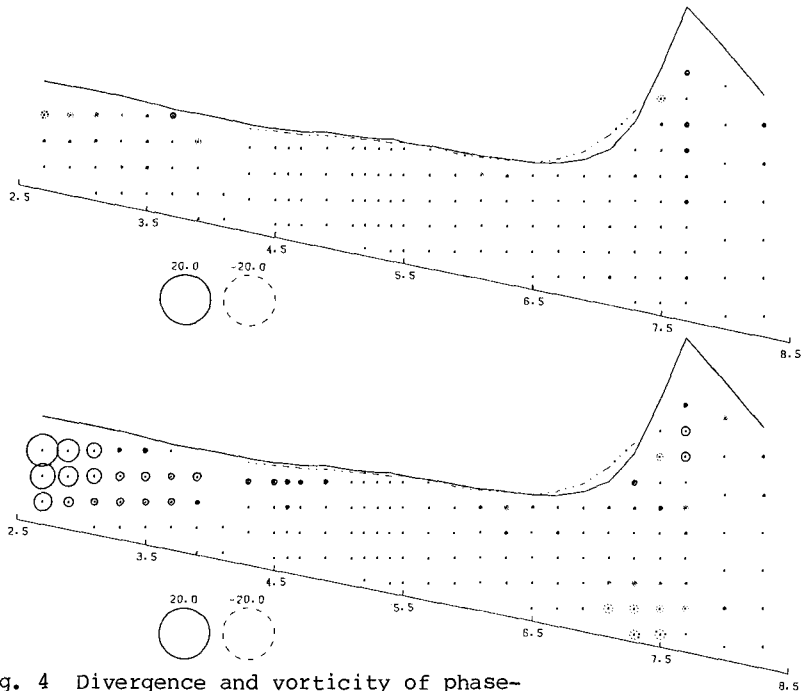
Fig. 4 Divergence and vorticity of phase-averaged velocity field. $(T_1=22)$ The diameters of the circles denote the magnitude. The solid circles indicate positive values while dotted ones do negative values. The positive divergence gives negative gradient of longshore velocity. The positive values of vorticity means anti-clockwise rotation of the water particles.

particle acceleration, Du/Dt is evaluated by using the relation $Du/Dt = \partial u/\partial t + u\partial u/\partial x + w\partial u/\partial z$. The partial differentiation with respect to time, t, is obtained numerically. Turbulence intensity, $\sqrt{(u')^2}$, is also calculated. The turbulence is defined as the difference between the instantaneous velocity and the phase averaged velocity. Thus obtained turbulence include the fluctuation of wave motion and may give overestimation as shown later. From the given spatial distribution of Eulerian velocity field, particle trajectories are traced numerically. Simple forward difference scheme is employed.

4 Results and discussion

Sixty one sequential diagrams of synthesized (phase averaged) velocity field with surface profile are carefully examined. With help of pictures taken during the experiments as well as the quantities $\nabla \cdot u$, $\nabla \times u$, Du/Dt and $\sqrt{(u')^2}$, it was revealed that there exist six typical stages in wave breaking, which are qualitatively described as follows.

I) Sharp crested wave, which a little inclines forward, advances in a uniform return flow. This is typically shown in Fig. 3, for the time sequence $T_i=22$. The initial phase $T_i=1$ is chosen arbitrary. The uniform return flow under the preceding trough is remarkable. The
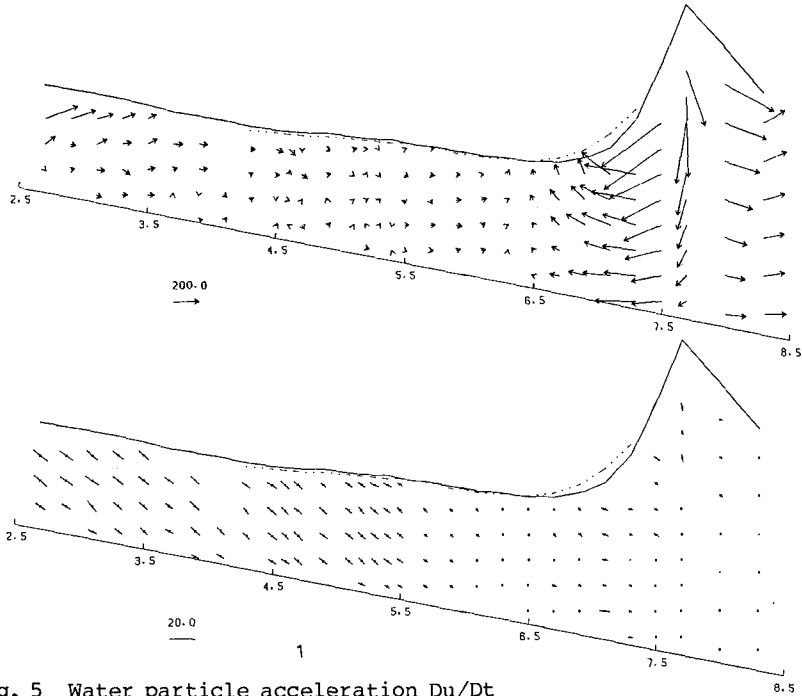

Fig. 5 Water particle acceleration Du/Dt and turbulence intensity $\sqrt{(u')^2}$. ($T_i=22$) Du/Dt is plotted as a vector. Turbulence intensity is plotted such that the length of the bars has the absolute value of turbulence $\sqrt{(u')^2+(w')^2}$ and the angle with the onshore horizontal line has the angle $\tan^{-1}(\sqrt{(w')^2}/\sqrt{(u')^2})$. If the turbulence is isotropic, the angle is 45 deg.
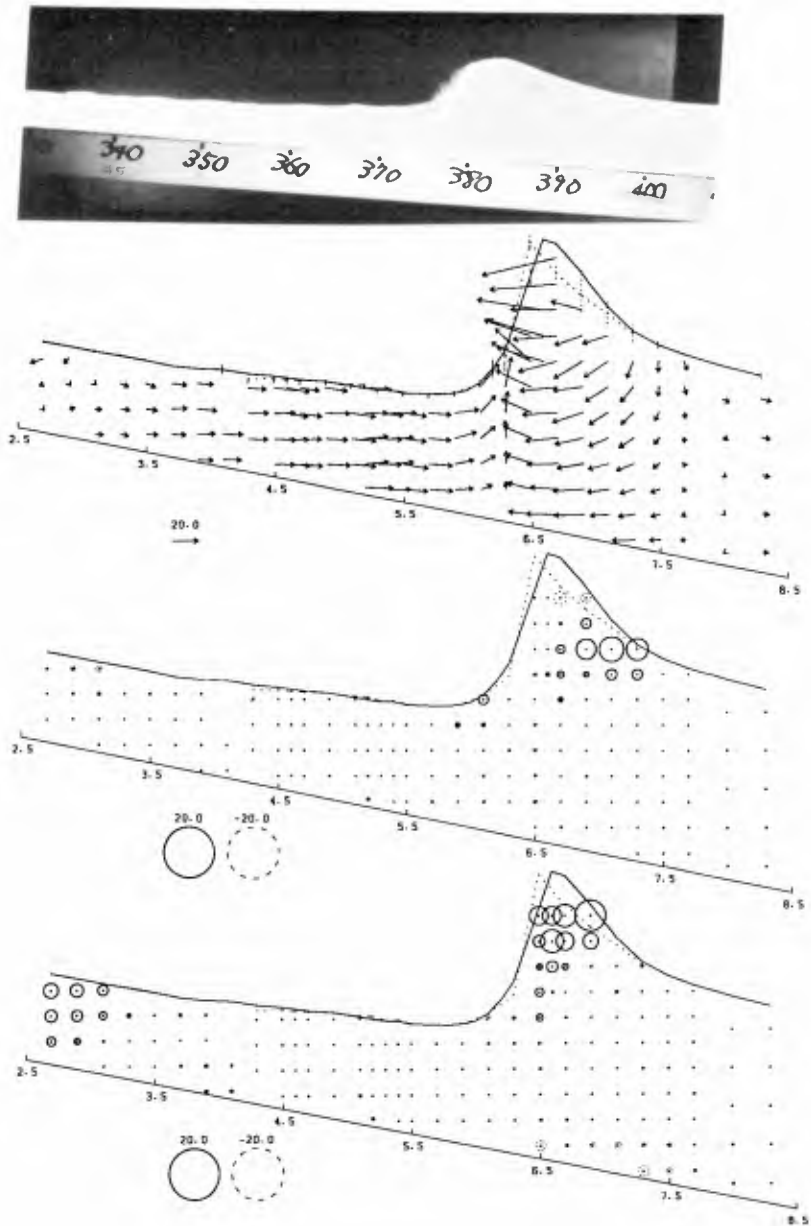
Fig. 6   Stage II, where the wave breaks. (T_i=33) Photo, velocity field, its divergence and vorticity.

foregoing wave has disappeared to the left. In Fig.4, the divergence
and rotation are shown for this phase T_i=22. The divergence is nearly
zero throughout the measuring area, assuring that the phase averaged
flow field is two-dimensional.   This may guarantee the reliability of
the experiment.   The non-zero vorticity, found far left, are the remains
of the vorticity generated by the plunging of the foregoing wave.
Whether the values of the divergence is negligibly small or not depends
on what to compare with.   Here the values are compared against the
significant values of the vorticity ($\equiv$30 s^{-1}) observed in this wave
breaking process.   The vorticity is twice the angular velocity of the
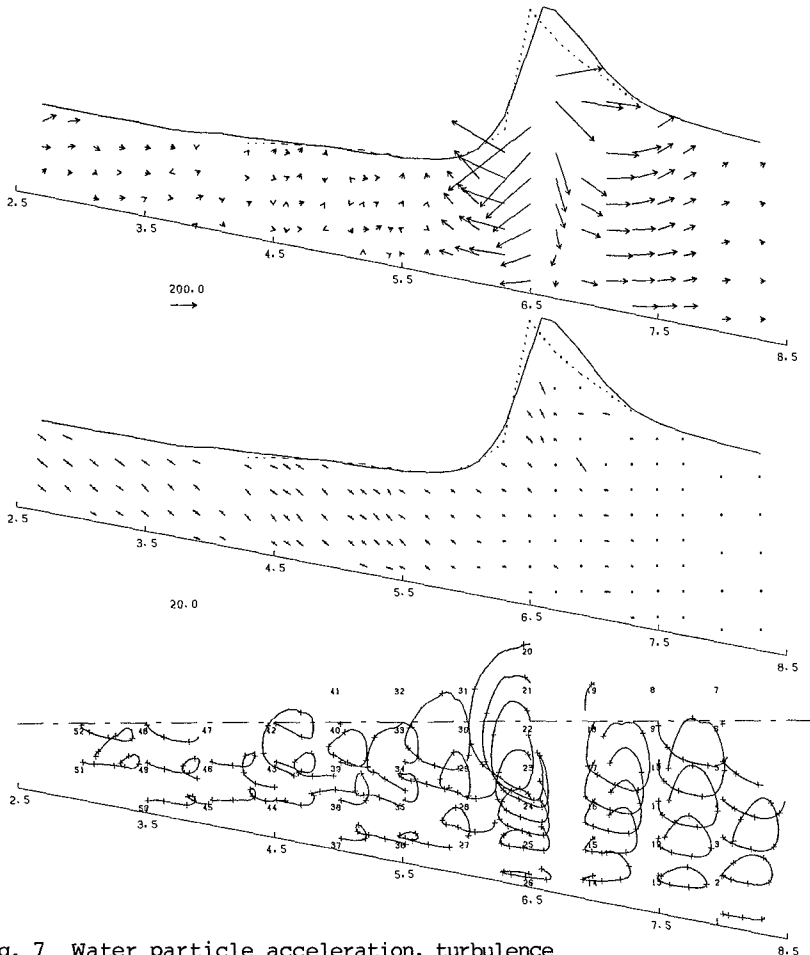rotational motion of a water particle.   The indicated values of 20 s^{-1}

Fig. 7 Water particle acceleration, turbulence
intensity and water particle trajectories. (T_i=33) The trajectories are
followed for one wave period.   The points near the number are the
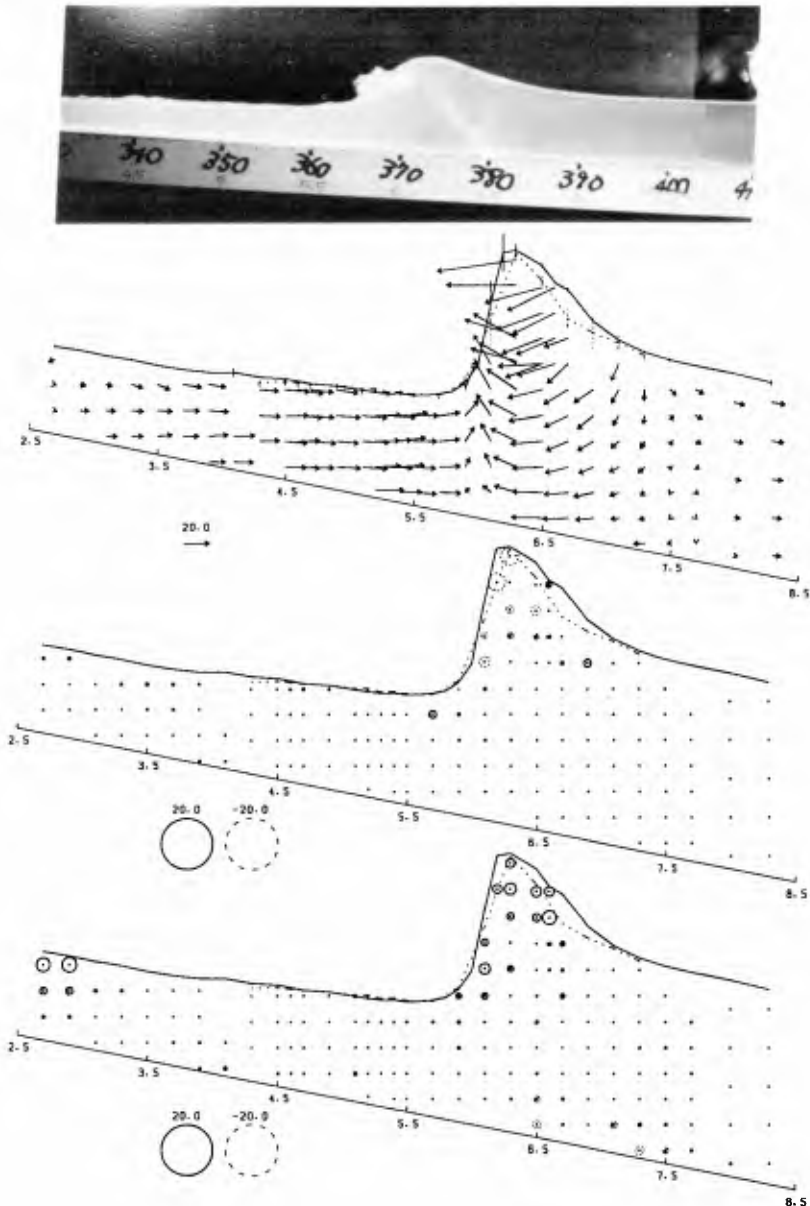stating positions at this instant.

Fig. 8 Stage III, where the breaking (overturning) wave travels.
(T_i=36) Photo, velocity field, its divergence and vorticity. The
plunging jet does not yet touch down.

in Fig. 4 means that the water particles rotate with the angular
velocity 10 s^{-1}.   Figure 5 shows the water particle velocity and
turbulence intensity for T_i=22. The water particle acceleration shows a
reasonable behaviour that particles are accelerated only when the wave
crest passes. The dynamics of the breaking wave appears to be quite
similar to that of a solitary wave. With respect to the turbulence
shown in Fig. 5, significant values are found only after the plunging
point. The large values under wave crest are due to the fluctuation of
wave motion as is indicated by the vertical bar on the surface profiles
in Fig. 3. This stage covers the period of time sequence number (15-32).
    II) The crest continues to become sharper and some part of its
front face finally becomes vertical. At this breaking moment, horizon-
tally converging and vertically upwelling flow beneath the vertical
front face is very remarkable as shown in Fig. 6. Stagnation point is
observed at the bottom of the upwelling flow. The maximum value of the
velocity measured, which is nearly horizontal, is 67 cm/s. This value
is likely to be underestimated as it is the maximum of the phase-
averaged ones. From the number plotted in Fig. 2, we have 83 cm/s for
wave crest propagation velocity, v_c, near this breaking point.
Considering that the point of maximum velocity lies within the fluid,
one can imagine that the real maximum velocity is nearly equal to v_c. It
is also shown in Fig. 6 that divergence and vorticity take non-zero
values around the top of the wave crest. The positive divergence behind
the crest results from the fact that the velocity vectors around there
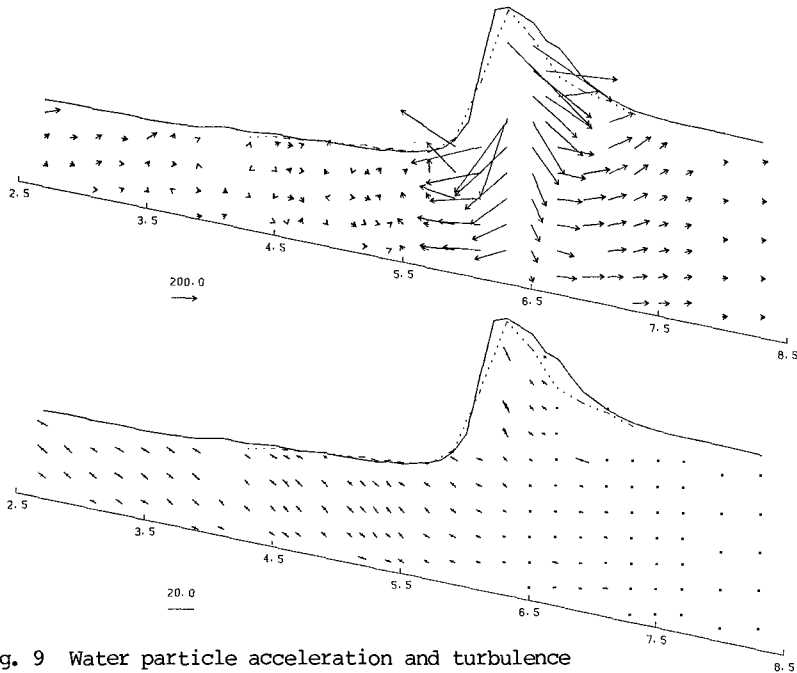do not show a smooth variation. Experimental errors due to very fast

Fig. 9 Water particle acceleration and turbulence
intensity for T_i=36.

movement of the breaking wave crest could be responsible for this false
(?) three dimensional feature. The positive vorticity at the top of the
wave crest is due to the higher nearly-horizontal velocities at the
points nearer to the surface. This generation of small vorticity is a
token of the breaking inception. Rotational motion at the top of a
nearly-breaking wave is also observed for a spilling-type breaker by
VanDorn & Pazan(1975). Vorticity far left still remain, decaying. In
Fig.7, the observed maximum vertical acceleration is 490 cm/s^2 in the
downward direction at the highest point measured beneath the crest.
Extaporation up to the surface may give the value of g=980 cm/s^2.

   III) The plunging jet is formed from a part of the sharp crest,
although the remaining part of the wave continues to propagate
independently. As shown in Figs. 8 and 9, the observed features are the
same for those of stage II in Figs. 6 to 7, except that the height of
wave crest is decreasing. (33-43)

   IV) The jet is plunging into the front face of the original wave,
hitting the surface as shown in Figs. 10 and 11. In this stage the wave
motion still holds its characteristic feature under the plunging jet.
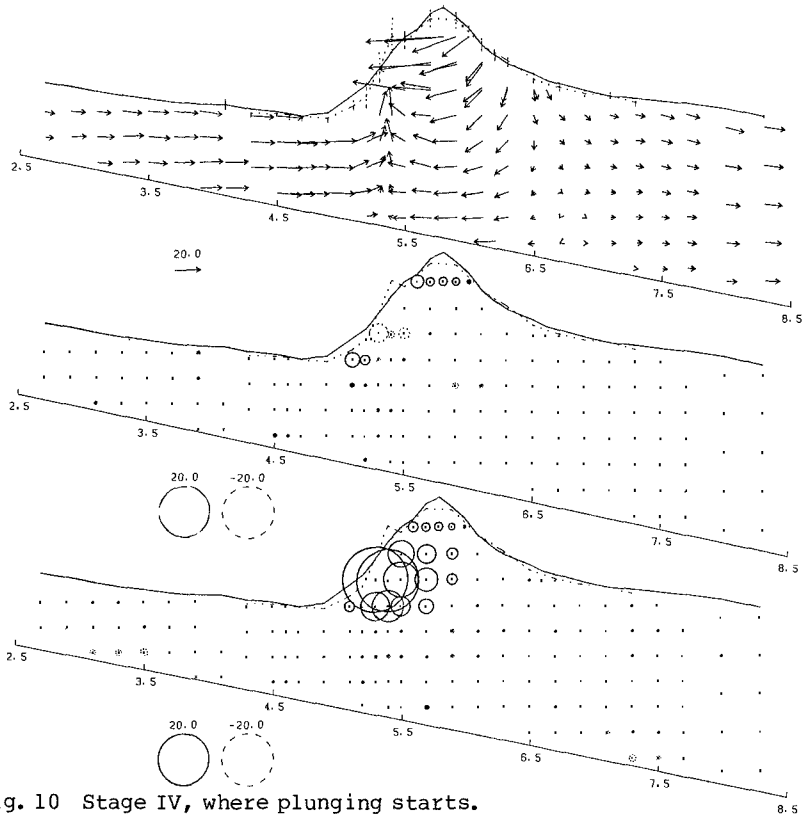This plunging moment is most clearly characterized by the beginning of

Fig. 10 Stage IV, where plunging starts.
(T_i=44) Velocity field, its divergence and vorticity.

the generation of large vorticity and turbulence near the surface at the
plunging point. The vorticity is generated by the strong shear near the
surface due to the plunging jet, which appears to flow over the surface.
At this stage the vorticity far left produced by the foregoing wave
disappears.   In Fig. 11 particle trajectories show that the surface
particles do not penetrate into water deeply, indicating that the
surface generated vorticity and turbulence do not easily reach the
bottom. It is noted that the vorticity exists almost only above the
wave trough level. On the other hand, the fluctuation of pressure may
produce turbulence even near the bottom.   (44-50)
      V)   Then the plunging jet produces a dead water region beneath the
plunging point but neither so-called horizontal roller nor offshoreward
propagating wave.   In Figs. 12 and 13 it appears that the plunging jet
bounce up over the dead water region. This process is described by as a
jet-splash motion Jannsen(1986) based on visual technique. It is
interesting to investigate how this bouncing process changes as the
breaking pattern differs.   As shown in Fig. 13 and others, turbulence
near the surface is likely to be isotropic, but very near the bottom,
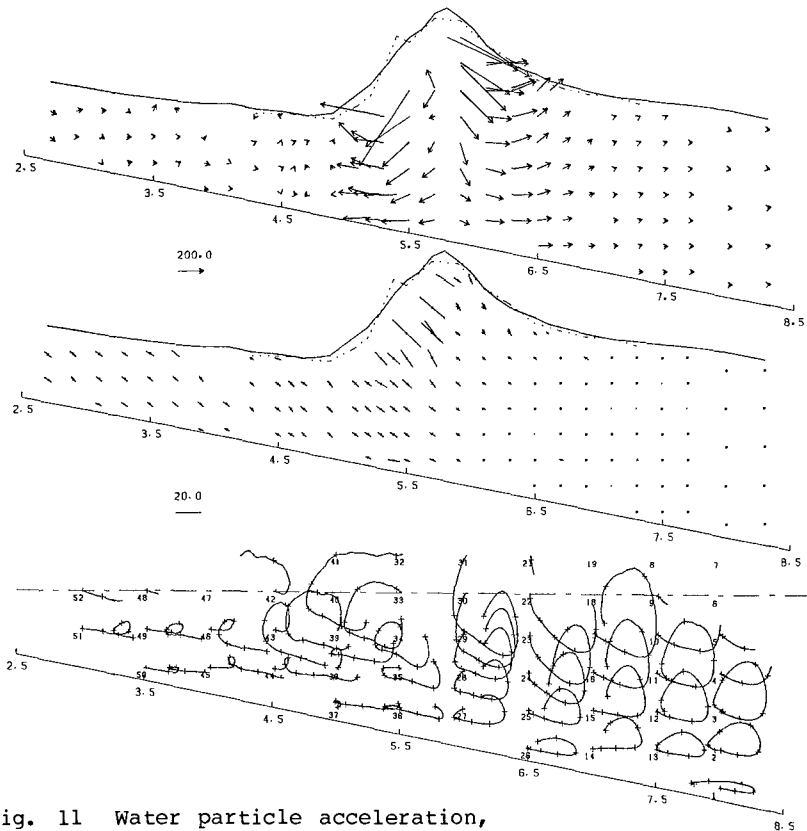turbulence in vertical velocity is naturally small.   (50-61)

Fig. 11   Water particle acceleration,
turbulence intensity, and trajectories for T_i=44.

VI) As shown in Fig. 14, bore-like motion is formed. The flow
field at the wave front is similar to that in Stage I as shown in Fig.3.
However the vorticity within and behind the bore-like wave exist
together with the turbulence. The rotational motion as well as the
turbulence is left behind as the crest propagates away.   (1-14)

5 Conclusions
     It is concluded that wave breaking is a phenomenon in which
irreversible motion of the jet-forming with small vorticity stands for
its inception and the plunging of the jet into the original wave causes
partial destruction of the original wave, resulting with the bore-like
motion. However the plunging jet may not penetrate into the interior of
water but bounce up over a dead water region and does not form either
the roller directly nor the outward-going waves. It also brings about
the turbulence together with the rotational motion with vorticity.

Acnowledgements
     I would like to give my special thanks to Mr. K. Sakata for his
assistance throughout every phase of this study.

Reference
Basco, D.R.(1985), A qualitative description of wave breaking, J. WPCOE,
     ASCE, 111, No.2, 171-188.
Hedges, T.S. and Kirkgöz, M.S.(1981), An experimental study of the
     transformation zone of plunging breakers, Coastal Eng., 4, 319-333.
Jansen, P.C.M.(1986), Laboratory observation of the kinematics in the
     aerated region of breaking waves, Coastal Eng., 9, 453-477.
Longuet-Higgins, M.S. and E.D. Cokelet(1976), The deformation of steep
     surface waves on water, 1. A numerical method of computation, Proc.
     Roy. Soc. Lond., A-350, 1-26.
Miller, R.L.(1976), Role of vortices in surf zone prediction:
     Sedimentation and wave forces, Soc. Econ. Paleontol. Mineralog.,
     Spec. Publ., No.24, 92-114.
Okayasu, A., T. Shibayama and N. Mimura(1986), Velocity field under
     plunging waves, to be published in this Proceedings.
Peregrine, D.H.(1983), Breaking waves on beaches, Ann. Rev. Fluid Mech.,
     15,149-178.
Peregrine, D.H. and I.A. Svendsen(1978), Spilling breakers, bores and
     hydraulic jumps, Proc. 16th Conf. on Coastal Eng., 540-550.
Stive, M.J.F.(1980), Velocity and pressure field of spilling breakers,
     Proc. 17th Conf. on Coastal Eng., 547-566.
VanDorn, W.G. and S.F. Pazan(1976), Laboratory investigation of wave
     breaking Part II: deep water waves, AOEL Rep. 71, Scripps Inst.
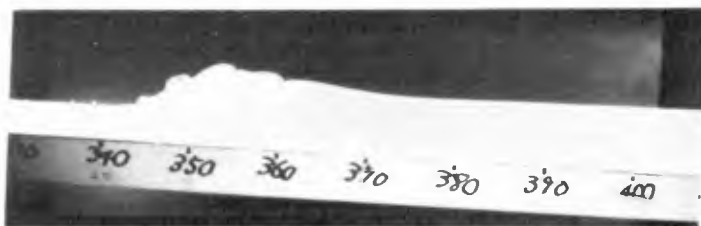   Oceanogr., Univ. Cali., San Diego, 106p.

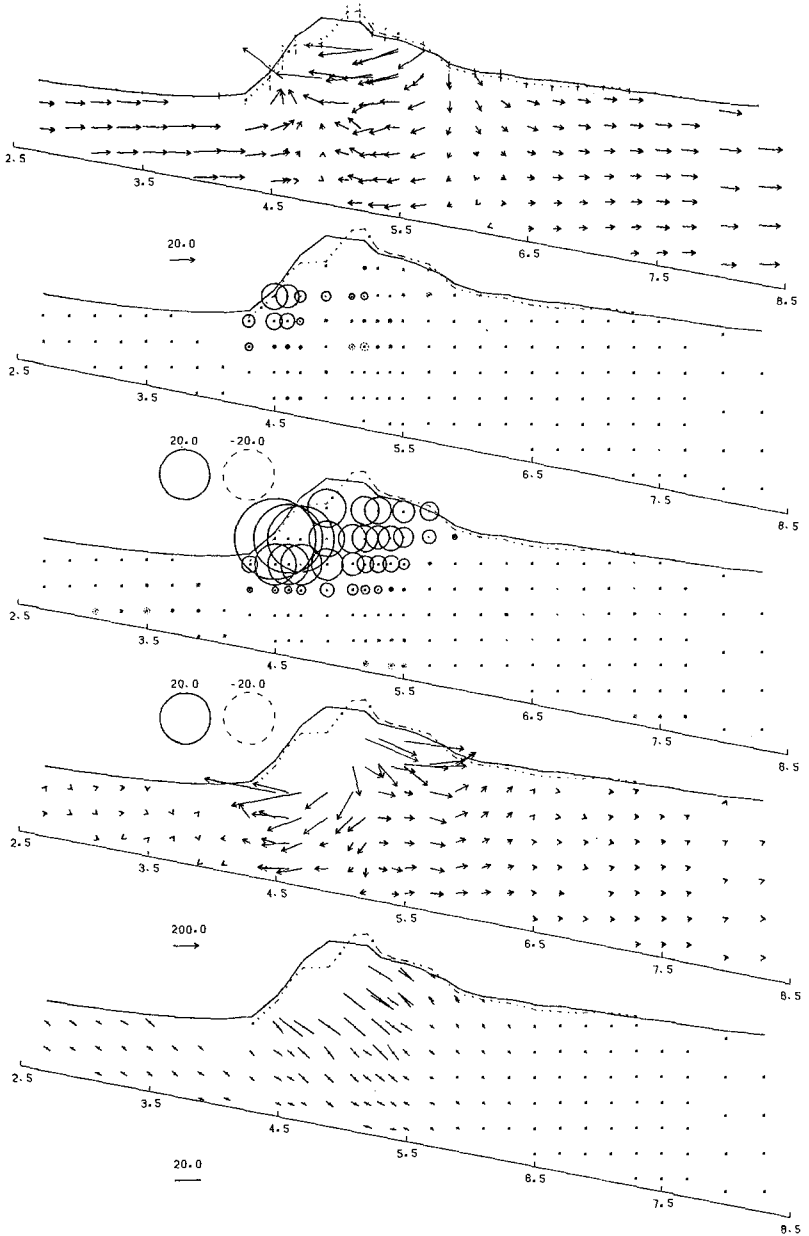Fig. 12   Stage V, where plunging jet is bouncing up.   Photo.

Fig. 13 Velocity field, its divergence and vorticity, water particle
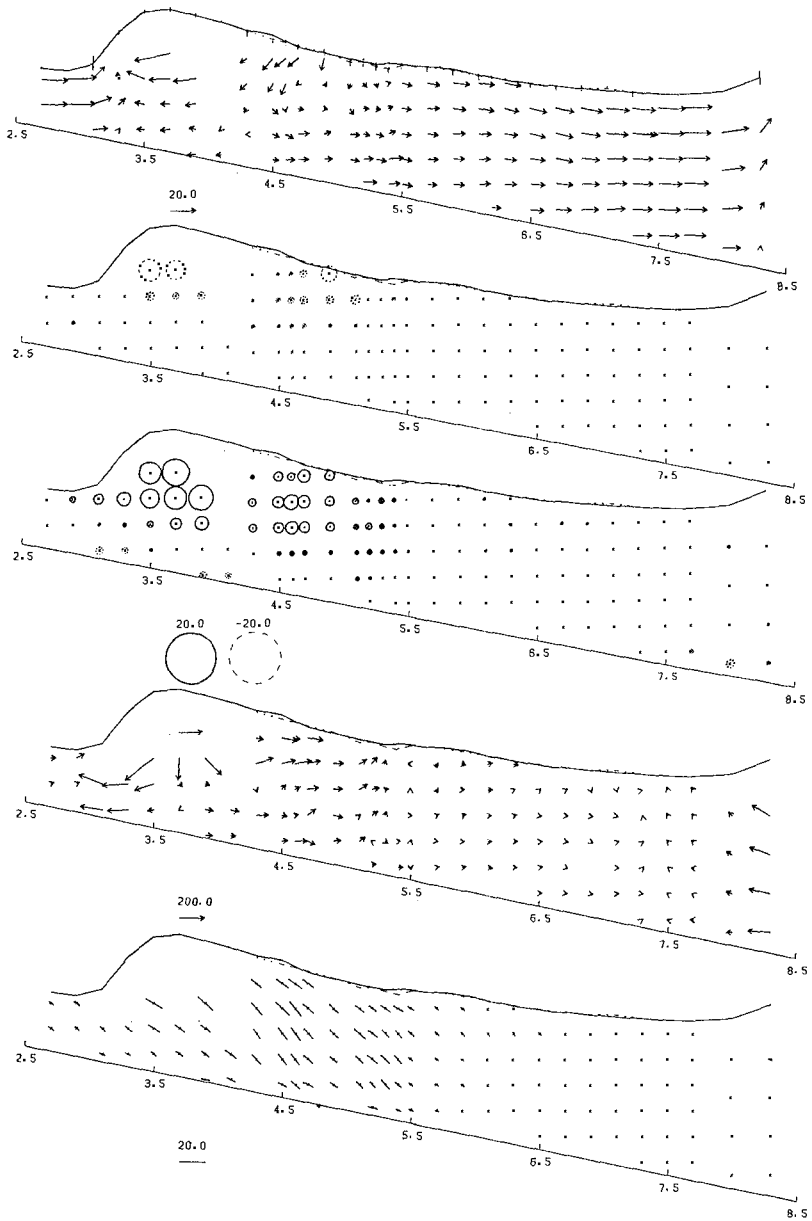acceleration and turbulence intensity. (T_i=51)

Fig. 14 Stage VI, where bore-like wave is formed. (T_i=6) Velocity field, its divergence and vorticity, water particle acceleration, and turbulence intensity.